JOURNAL OF COMPUTATIONAL PHYSICS 108, 180–196 (1993)

A Novel Technique for the Numerical Simulation of Hot Collision-Free Plasma; Vlasov Hybrid Simulation

D. NUNN

Department of Electronics and Computer Science, University of Southampton, Hampshire SO9 5NH, United Kingdom

Received November 13, 1991; revised October 12, 1992

This paper reports a simple novel technique for the numerical simulation of hot collision-free plasmas. The method is termed Vlasov hybrid simulation (VHS). A time varying phase space simulation box and grid are defined, and the phase fluid within the box is filled with simulation particles. The distribution function F (or δF) is defined on the phase trajectory of each particle. At each timestep F (or δF) is *interpolated* from the simulation particles onto the phase space grid. Particles are followed continuously until exiting from the phase box and are not constantly recreated at phase space grid points. The algorithm is very efficient, stable, and has low noise levels. Distribution function fine structure is tolerated and the formalism does not require diffusion of the distribution function. The VHS method is particularly valuable when the flux of phase fluid across the phase box boundary is significant. In this case VHS codes have a *dynamic* population of particles—giving great efficiency gains over PIC codes with fixed particle populations. The VHS method has been applied to the numerical simulation of triggered VLF emissions in the magnetosphere and gives results in close agreement with observations.

1. INTRODUCTION

This paper will introduce a novel method for the numerical simulation of hot collision-free plasmas. The method is termed Vlasov hybrid simulation (VHS), since it uses information derived from particles in order to construct the distribution function at every timestep. The formalism is a very general one for the solution of the Vlasov/Maxwell equations and may be applied to any collision-free plasma problem, where the resolution of the particle distribution function in velocity space is important. The methodology is strictly collision-free. However, collisional affects and velocity space diffusion could be introduced but not easily or conveniently.

Application areas for the VHS method are extremely diverse. The demonstrator application in this paper will be the numerical simulation of triggered VLF emissions in the earth's magnetosphere, the VHS method being extremely well suited to wave particle interaction problems, particularly those in inhomogeneous media. Other obvious application areas in space physics are nonlinear Landau damping, ion acoustic double layers, nonlinear ion cyclotron resonance, and simulations of cometary wakes, ion releases, and shock waves. There are expected to be numerous applications to fusion and industrial plasmas in cases where the plasma may be treated as effectively collision-free.

It will be shown that the VHS method has significant advantages over PIC codes [1] and also over other Vlasov codes. The most significant positive features are:

(a) VHS is a very stable algorithm.

(b) The technique has very low noise levels.

(c) Distribution function fine structure is handled easily.

(d) The method makes very efficient use of particles, particularly when $\delta F \ll F_0$.

(e) No numerical diffusion of distribution function is needed in order to attain stability.

(f) The VHS technique is particularly effective when the flux of phase fluid at the boundary of the phase space simulation box is significant. The methodology allows a dynamic population of simulation particles in which redundant particles may be discarded from the simulation and new particles inserted into the phase fluid as required.

2. BASICS

The Maxwell/Vlasov set of equations for a collision-free plasma are

$$\nabla \times \mathbf{E} = -\frac{\partial \mathbf{B}}{\partial t}; \qquad \nabla \cdot \mathbf{B} = 0$$
$$\nabla \cdot \mathbf{E} = \rho/\varepsilon_0; \qquad \nabla \times \mathbf{B} = \mu \mathbf{j} + \frac{1}{c^2}\frac{\partial \mathbf{E}}{\partial t} \tag{1}$$

and

$$\left(\frac{\partial}{\partial t} + \mathbf{v}\cdot\frac{\partial}{\partial \mathbf{x}} + \frac{q_\alpha}{m_\alpha}(\mathbf{E} + \mathbf{v}\times\mathbf{B})\cdot\frac{\partial}{\partial \mathbf{v}}\right) F_\alpha = \frac{d}{dt} F_\alpha = 0, \tag{2}$$

0021-9991/93 $5.00

where it is assumed that M particle species are present. Plasma charge density ρ and plasma current $\mathbf{J}$ are given by

$$\left.\begin{matrix} J \\ \rho \end{matrix}\right\} = \sum_{\alpha=1}^{M} q_\alpha \int_{\mathbf{v}} \left\{\begin{matrix} \mathbf{v} \\ 1 \end{matrix}\right\} F_\alpha \, d\mathbf{v}. \tag{3}$$

It should be noted that it may not be appropriate for all particle species to be treated by VHS. Some species may be described by fluid equations. Some components of the plasma may be cold plasma or cold beams, better described analytically or by PIC codes. The remainder of this paper will consider only one species of particle to be described totally by VHS.

The plasma is described as a Vlasov fluid occupying phase space of appropriate dimensionality n. Granularity of the phase fluid will be ignored. The unperturbed or initial distribution function F_0,

$$F_0(\mathbf{x}, \mathbf{v}) = F(\mathbf{x}, \mathbf{v}, t = 0), \tag{4}$$

is required to be a regular and well-behaved function of the phase coordinates $\mathbf{x}$, $\mathbf{v}$. Well-separated discontinuities are permissible but delta function-like singularities (corresponding to cold beams) are not allowed. Where cold beams are present these must either be given a finite temperature to incorporate them into the VHS formalism or treated separately with a PIC code.

3. THE PHASE SPACE SIMULATION BOX

The first step is to construct a phase space simulation box (PSB) which covers the region of phase space deemed significant for the problem at hand. In general the PSB will be a *function of time* as the simulation progresses. For example, in a resonant wave particle interaction problem the phase box would cover the range of velocities resonant with the current wavefield. As the wavefield spectrum changes during the simulation, so will the range of resonant velocities and thus the phase box will move.

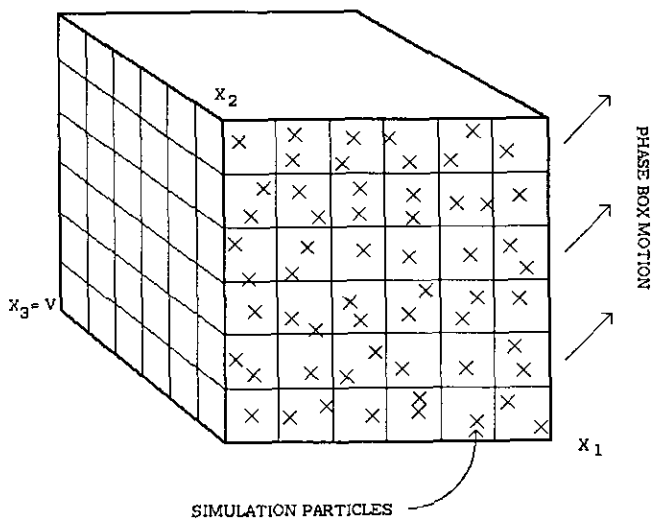

FIG. 1. Phase space simulation box and grid indicating possible box motion.

Next, a phase space grid is defined to fill the phase simulation box. Henceforth, we shall assume a regular grid with constant elementary volume $d\Gamma = d\mathbf{x} \cdot d\mathbf{v}$. It should be noted that the VHS technique is well able to accommodate grids of varying density $d\Gamma^{-1}$, and indeed adaptive grids. Figure 1 is a sketch of the phase box, showing the grid, simulation particles, and indicating its possible motion.

4. SIMULATION PARTICLES

The phase space simulation box is evenly filled with simulation particles (SP's) at the start of the simulation ($t = 0$). At each time step every particle is pushed according to the usual equations of motion:

$$\dot{\mathbf{x}} = \mathbf{v} \tag{5}$$

$$\dot{\mathbf{v}} = q/m(\mathbf{E} + \mathbf{v} \times \mathbf{B}). \tag{6}$$

Each particle trajectory is continuously followed until it leaves the simulation box. Trajectories are not continuously restarted at phase space grid points as in the paper by Denavit [2]. New trajectories are continually started at the phase box boundary.

Now each SP is embedded in the Vlasov phase fluid and moves with it. By Liouville's theorem each SP conserves its value of distribution function $F(\mathbf{x}, \mathbf{v}, t)$. The values of F (or δF) are defined on the phase trajectories of the simulation particles. Thus during the simulation the value of the distribution function is known at a large number of points in the phase box which are the locations of the SP's. The function of the SP's is solely to provide *information*. At each timestep this information is used to construct the particle distribution function on the fixed phase space grid and thus make *estimates* of the zeroth and first moments of F—which are, of course, plasma charge density and current density.

At each timestep we require the *interpolation* of the values of the distribution function F_l from the particles onto the fixed phase space grid, giving grid values $F_{ijk\ldots}$. This process of interpolation is quite different from that in PIC codes and other Vlasov codes, where a charge/current or, indeed, a distribution function is *assigned* or distributed to the neighbouring grid points.

Once a distribution funcion $F_{ijk\ldots}$ is defined on the fixed phase space grid, estimates of charge ρ and current $\mathbf{J}$ are easily obtained. For the 6D cases we have

$$\left.\begin{matrix} J \\ \rho \end{matrix}\right\}_{ijk} = q \, d\Gamma \sum_{lmn} \left\{\begin{matrix} v \\ 1 \end{matrix}\right\}_{lmn} F_{ijklmn}. \tag{7}$$

With the charge and current fields defined on the spatial grid the electromagnetic fields may be pushed using standard fieldpush techniques.

In many plasma simulation problems it might be more convenient to define the quantity δF on each simulation particle phase space trajectory, where

$$\delta F(\mathbf{x}, \mathbf{v}, t) = F(\mathbf{x}, \mathbf{v}, t) - F_0(\mathbf{x}, \mathbf{v}) \tag{8}$$

whence

$$\frac{d}{dt}\delta F = -\mathbf{v}\frac{\partial F_0}{\partial \mathbf{x}} - \frac{q}{m}(\mathbf{E} + \mathbf{v}\times\mathbf{B})\frac{\partial F_0}{\partial \mathbf{v}}. \tag{9}$$

The demonstrator application defines δW for each SP, where

$$\frac{d}{dt}\delta W = -q\mathbf{E}\cdot\mathbf{v}. \tag{10}$$

In the VHS formalism the distinction between defining F or δF on the phase space trajectories of SP's is fairly trivial, and hence the VHS method may be regarded as one in which δF is pushed forwards in time.

A final comment will be made in this section. The VHS method is **not** the same as a PIC code in which particles are weighted according to the initial distribution function. The interpolation procedure and also the treatment of the phase box boundaries ensure that the manner in which available information is treated is quite different.

5. INTERPOLATION OF DISTRIBUTION FUNCTION FROM PARTICLES TO THE PHASE SPACE GRID

Clearly for the VHS method to be viable we need a simple and efficient method for the interpolation of F from the particles onto the fixed phase space grid. Figure 3 shows a representation of phase space of dimensionality $n = 2$. Using a derivative of the method of area weighting a suitable expression for the value of distribution function F_{ij} at grid point ij is

$$F_{ij} = \left\{\sum_{l'=1}^{l} \alpha_{l'} F_{l'}\right\} \Big/ \left\{\sum_{l'=1}^{l} \alpha_{l'}\right\}, \tag{11}$$

where the weight factor $\alpha_{l'}$ for the l'th particle is given by

$$\alpha_{l'} = \left\{A_1 \Big/ \sum_{j=1}^{4} A_j\right\}. \tag{12}$$

The sum is taken over all l simulation particles within the four square area surrounding the grid point in question. The above technique will give a very low noise level in F_{ij} and is simple and easy to encode.

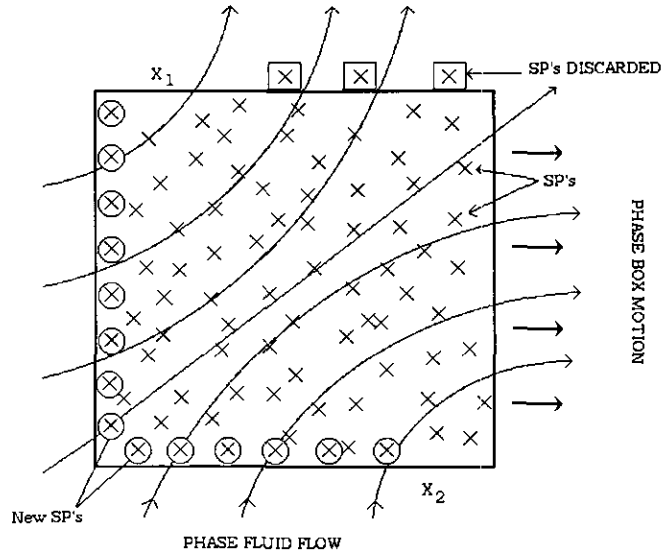

FIG. 2. Representation of a two-dimensional phase box showing phase fluid flow and particle management.

A small number of grid points ij ($< 1\%$) will not have any SP's within the surrounding four square area. In these cases F_{ij} has to be calculated by linearly interpolating values of F from neighbouring grid points.

The expressions in Eqs. (11) and (12) are readily generalised to the case of n-dimensional phase space. Figure 4 shows a representation of n-dimensional phase space with elementary volume $d\Gamma = \prod_{i=1}^{n} dx_i$. A total of 2^n hypercubes will be adjacent to grid point $ijk\ldots$. If a total of l particles lies within this volume of phase space then a suitable expression for $F_{ijk\ldots}$ is given by

$$F_{ijk\ldots} = \left\{\sum_{l'=1}^{l} \beta_{l'} F_{l'}\right\} \Big/ \left\{\sum_{l'=1}^{l} \beta_{l'}\right\}, \tag{13}$$

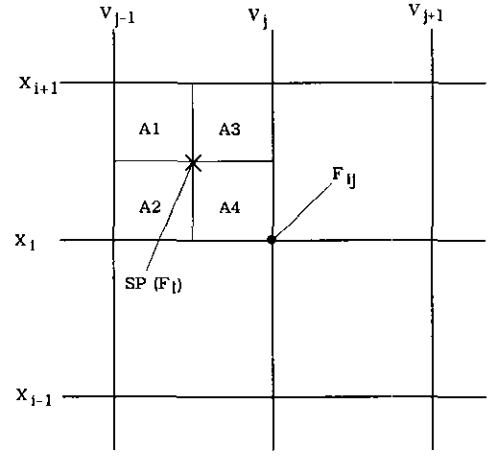

FIG. 3. Interpolation of distribution function F_1 from particles to the fixed phase space grid—2D case.

where the weighting factor for particle l' may be defined by

$$\beta_{l'} = \prod_n (dx_n - \delta x_n^{l'}) \Big/ \prod dx_n. \tag{14}$$

Here $\delta x_n^{l'}$ defines the vector from the grid point $ijk\cdots$ to the l'th particle.

Obviously a wide variety of definitions for the weighting factor are possible and most of these will give a reasonable performance. (See, for example, Okuda and Cheng [20].) The greatest need is for an algorithm that gives simple, vectorisable, and economical code. There is some scope for theoretical research and simulation in order to optimize these weighting factors.

6. THE REQUIRED DENSITY OF SIMULATION PARTICLES IN PHASE SPACE

The situation is now as follows. The phase box is a function of time and is filled by a fixed grid. Simulation particles are embedded in the phase fluid within the phase box and at each timestep the distribution function is interpolated from the particles onto the fixed grid, enabling the $\mathbf{J}/\rho$ fields to be calculated. We now express the basic requirement of the VHS algorithm which we will term the *fundamental density law*. This may be stated as follows:

> For a phase space of dimensionality n the probability p that any grid point has at least *one* simulation particle in the surrounding 2^n grid hypercubes must be very close to unity—say $1.0 > p > 0.995$.

The question then arises—what average density of SP's in the phase fluid ensures that the fundamental density law will be satisfied? We first note from Liouville's theorem that the density of SP's in the phase fluid $\hat{\rho}$ is conserved following a particle and thus the flux of SP's in phase space is divergence-free. There is no tendency for SP's to bunch and leave grid points uncovered. Uncovered grid points are most likely to occur on the boundaries of the phase box and these near boundary grid points are best omitted from the computation of $\mathbf{J}$ and ρ.

The demonstrator application described later in the paper reduces to a 2D phase space problem. Numerical experimentation revealed that an average density of $\hat{\rho} = 1.2/d\Gamma$ gave a grid point "coverage" of 99.5%. It is easily shown that for an n-dimensional phase space we need a simulation particle density of

$$\hat{\rho} \geqslant \hat{\rho}_0 = 4.8/(2^n\, d\Gamma). \tag{15}$$

With increasing dimensionality fewer SP's are needed per elementary volume $d\Gamma$, a fact that has been noted in connection with PIC codes. So for a 6D phase space a density of $\hat{\rho} = 0.075/d\Gamma$ would suffice.

In some problems such as hot beam excitation there will be regions of phase space where $F = 0$. Simulation particles need not be placed in these regions. It is only necessary to increase SP density somewhat to $1.2\hat{\rho}_0$ in regions where $F \neq 0$, and then all phase space grid points $ijk\ldots$ that have no SP's in the surrounding 2^n hypercubes may be regarded as having $F_{ijk\ldots} = 0$.

We now emphasise an important point. The only criterion governing SP density in the phase fluid is the fundamental density law. Higher densities than the approximate limit $\hat{\rho}_0$ defined above are quite permissible. Increased particle density results in more computational workload, but fewer missed grid points, more accurate estimation of $\mathbf{J}$, ρ, and better averaging over distribution function fine structure.

Another feature of the VHS algorithm is that it does not matter if the density of particles in the phase fluid is highly variable, as long as it never falls below the minimum levels. This is a feature unique to VHS that is a direct result of the interpolation procedure. We shall see that this makes it relatively easy to deal with a flux of phase fluid into and out of the phase space box. PIC codes and other Vlasov codes are all highly sensitive to particle density in phase space, and these codes usually have great difficulty in dealing with fluxes at the phase box boundary.

It is useful at this point to give an estimate of the number of particles required by a VHS simulation of a "typical" problem. Consider a simulation with one spatial dimension with 1000 grid points, and three velocity dimensions with grid dimensions $30 \times 30 \times 30$. Then we have $N_t \sim 30^3 \times 1000 \times 4.8/16 \sim 8M$, an entirely achievable figure with modern supercomputers.

7. PARTICLE CONTROL

Any VHS code needs to have software that controls the particle population and maintains the density $\hat{\rho}$ of SP's everywhere above the minimum level $\hat{\rho}_0$. Over parts of the phase box surface the nD "velocity" vector $\dot{\mathbf{X}}$ of the phase fluid relative to the velocity of the boundary itself is directed outwards. Over this surface phase fluid is flowing out of the phase simulation box. Simulation particles embedded in the fluid leave the box and by implication find themselves in a region of phase space that is "unimportant." Such particles are providing information not required and are *discarded* from the simulation. Thus VHS allows for a free flow of phase fluid out of the simulation box. Such phase fluid still "exists" but is not monitored and is not used to estimate the $\mathbf{J}/\rho$ fields.

Conversely parts of the phase box surface will see phase fluid flowing *in*. Clearly new SP's must be inserted into this

phase fluid. The best way of doing this is as follows. At each timestep all grid points on or near the phase box boundary are examined. Where there are no particles within adjacent hypercubes a new particle is inserted into the phase fluid. The exact position where new particles are placed will determine the resulting density of SP's in this inflowing phase fluid. Figure 2 gives a pictorial view of the phase box and the management of simulation particles. The VHS algorithm is on the whole very simple and trouble-free, but this can be one aspect which needs care. In the demonstrator application it was nevertheless found that controlling particle densities was quite easily achieved.

To summarise, the phase box is filled with particles at $t=0$. Each particle trajectory is followed until it leaves the phase box, and new SP's are continually created at the box boundary where fluid is flowing in. We thus see that the total number of particles N_t in the simulation at any one time is variable. The particle population is *dynamic* and continually changing. This can result in great increases in efficiency for some problems. In the demonstrator application particles leaving the phase box are those that have fallen out of resonance with the current wavefield. New particles introduced drift into resonance with the wavefield during their traversal of the phase box.

Since the total number of particles N_t can vary, a VHS code needs to keep N_t within reasonable bounds, say,

$$Nc\hat{\rho}_0 < N_t < 1.3Nc\hat{\rho}_0, \tag{16}$$

where Nc is the number of hypercubes in the phase box. If N_t falls too low, inaccuracy will increase and uncovered grid points will result. The solution is to create extra SP's in the interior of the phase box at grid points that have few nearby particles. If N_t becomes too large the program will slow up,

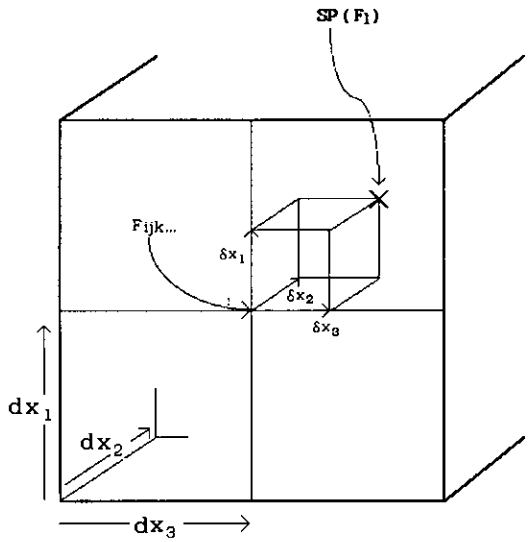

FIG. 4. Interpolation of distribution function F_1 from particles to the phase space grid—schematic representation for n-dimensional case.

and there will be a danger of overflow in arrays holding particle variables. Again the remedy is to remove SP's from the interior of the phase box at grid points where the number of nearby particles is large. In the demonstrator application it was found that these measures were rarely necessary and total particle numbers were adequately controlled by careful insertion of new particles at the boundary.

At internal boundaries inside the phase box where grid density $d\Gamma^{-1}$ changes it will also be necessary to create or remove particles depending upon the direction of flow of phase fluid.

There will exist a wide variety of problems where flux of phase fluid into and out of the phase box is negligible and where $F \sim 0$ on the phase box boundary. In this case the simulation may proceed with a *fixed* population of particles, provided that the initial density is somewhat raised to $\sim 1.2\hat{\rho}_0$ so that grid points with no local SP's may be safely assumed to correspond to $F=0$.

8. VALUES OF DISTRIBUTION FUNCTION FOR SIMULATION PARTICLES

At $t=0$ simulation particles are given a value for distribution function of F_0 ($\delta F=0$), where F_0 should be self-consistent with the presumed initial fields.

The previous section explains how new simulation particles have to be inserted into the phase fluid at the phase box boundary. The question immediately arises—what value of distribution function should be assigned to these new particles? A reasonable choice is to put $F=F_0$, the unperturbed initial value for distribution function (i.e., $\delta F=0$, $\delta W=0$). For many problems this will be quite sufficient. If the simulation turns out to be unduly sensitive to the choice of F for new particles this is probably symptomatic of a phase box that is too small.

In certain cases a better value for F for new particles may be available. In the demonstrator application, for example, a linear expression for δF may be derived from the electromagnetic field history of the simulation. Where a new particle is inserted into the interior of the phase box an initial value for F is readily secured by interpolating from neighbouring grid values $F_{ijk\ldots}$.

9. SOME COMMENTS ON DISTRIBUTION FUNCTION FINE STRUCTURE

In many plasma simulations, as time progresses the distribution function F may develop fine structure in phase space. For example, this occurs in nonlinear Landau resonance where resonant particles make many oscillations in the potential trap. Usually distribution function fine structure does not have a great deal of physical significance

since during the evaluation of $\mathbf{J}/\rho$ it will be averaged out. However, fine structure can be a considerable nuisance for Vlasov simulation codes. Other Vlasov simulations such as that of Denavit [2] and Cheng and Knorr [3] need to be stabilised by diffusive terms that smooth out fine structure. The VHS method, however, is intrinsically stable against distribution function fine structure since no attempt is made to evaluate the derivatives of F in phase space. The VHS method does not diffuse the distribution function. This is considered neither desirable nor necessary.

The only effect of fine structure on the VHS algorithm is a decrease in the accuracy of the estimation of $\mathbf{J}/\rho$. Such errors may be reduced by either employing a finer phase space grid or increasing the density of SP's. Such measures will not usually be necessary.

10. CONSERVATION OF ENERGY AND MOMENTUM

A few remarks will be made here concerning conservation of energy and linear momentum. In the case of PIC codes one has a closed system of fields and particles, and one is in a position to demand that the entire set of equations governing the plasma simulation conserves total energy and linear momentum. A VHS Vlasov code, however, is not a closed system. Expressions for momentum and energy balance involve regions of phase space outside the current phase space simulation box and would require knowledge of phase fluid no longer being monitored.

The immediate aim of the VHS technique is to estimate the $\mathbf{J}/\rho$ fields as accurately and efficiently as possible. In the limit that $\mathbf{J}$ and ρ are completely accurate then the VHS code will conserve energy and momentum— provided, of course, that the field and particle push equations are conservative of these quantities. In reality $\mathbf{J}$ and ρ will have stochastic errors which will result in nonconservation of energy and momentum. Further research needs to be done in this area.

11. PREVIOUS VLASOV SIMULATIONS

In the 1970s and 1980s a number of papers were written on Vlasov simulations—usually problems with one spatial dimension. Successful results were obtained and many authors commented on the potential benefits of the Vlasov approach to the numerical simulation of plasmas.

Two key methods stand out in the literature—that of Cheng and Knorr [3] and Denavit [2]. These two methods are quite different from each other and from the method described in this paper. The approach of Cheng and Knorr is to numerically integrate the Vlasov equation on a phase space grid. Particles are not used at all in this process. Because of distribution function fine structure (filamentation) the numerical procedure is very prone to instability and stabilisation is only achieved by an unphysical numerical smoothing of the distribution function. The actual algorithm to step F forward in time is very complex and computationally expensive. Related algorithms and splitting schemes by Boris [4] and Boris and Book [5] are also very complex. The Cheng and Knorr method should, in principle, cope with any phase box boundary condition and allow for free entry and exit of phase fluid. This aspect was not discussed in their paper although it seems that correct application of boundary conditions could be quite difficult. Cheng and Knorr applied their novel technique to the nonlinear one-dimensional Landau resonance problem and reported the method to be highly accurate and efficient.

Other authors have used Cheng and Knorr's approach to good effect. Chanteur [6] performed very successful simulations of ion acoustic double layers, and Bertrand *et al.* [7] reported successful Vlasov simulations using the method.

By constrast Denavit [2] uses particles in order to time advance the distribution function. Particles are started off at phase space grid points and are assigned appropriate values of F. After M timesteps the value of F for each particle is assigned to the nearest grid points (*not* interpolated as in VHS). This effects a reconstruction of the distribution function. This reconstruction process invokes phase space diffusion which serves to eliminate fine structure and keeps the whole algorithm stable. In the limit of $M \to 1$ Denavit reconstructs every timestep, which gives strong diffusion in phase space. In this limit, flux of phase fluid into and out of the phase box can be accommodated. Many of Denavit's simulations use $M = 10$ which gives a hybrid solution, partly Vlasov, partly PIC. This mode of operation makes fluid flux across the phase box boundary difficult to accommodate. In the limit $M \to \infty$, the distribution function is never reconstructed and the method reverts to a PIC code in which particles are weighted by the distribution function. Denavit's method has been very effectively applied to two stream instability problems and to nonlinear Landau resonance (bump in tail instability) [2, 8–10].

Another Vlasov technique is the so-called "δF algorithm." This was first described by Tajima and Perkins [21] and is covered in Tajima [22]. This method was developed by Kotschenreuther [11, 24] into a highly successful code, some results of which are presented in Kotschenreuther [23]. In the above article another version of the δF algorithm due to Wong is described and is claimed to be virtually "noise-free." Additional development of the δF algorithm may be found in Beyers [25], Dimits *et al.* [26], and Barnes *et al.* [27].

The δF method is as follows. The quantity δF is computed for each simulation particle. Phase space is filled with particles each occupying a known volume $d\mathbf{x} \cdot d\mathbf{v}$. At each timestep the quantity $(\mathbf{v}\, \delta F \cdot d\mathbf{x} \cdot d\mathbf{v})$ is *assigned* to the nearest spatial grid points, and hence $\mathbf{J}/\rho$ fields are

calculated. The method resembles that of Denavit with no reconstruction and also has PIC features except that δF is pushed. The method has been applied to the simulation of the 1D Vlasov equation and also to a purely magnetic electron drift kinetic ampere law. The Vlasov code was found to considerably outperform corresponding PIC codes. Kotschenreuther [11] pointed out that for many fusion problems $\delta F \ll F$, and in these cases PIC codes are highly noisy and very inefficient.

Despite superficial resemblances between the δF algorithm and the VHS algorithm, the two are quite different. In the δF algorithm particles are distributed evenly in the phase fluid, and the phase volume associated with each particle is presumed to be preserved during the simulation. Consequently no velocity grid is required, and $\{\delta F \mathbf{v}\, d\mathbf{x}\, d\mathbf{v}\}$ is **distributed** to the nearest grid points as in PIC codes. By contrast, with VHS, particle density in the phase fluid is freely variable above a certain minimum and F (or δF) **must be** truly *interpolated* onto a velocity space grid. This different formalism is, of course, required if only a portion of phase space is to be resolved and fluxes across the phase box boundary are to be accomodated.

12. ADVANTAGES OF VHS COMPARED TO PIC CODES

The VHS algorithm has many advantages when compared with PIC codes. For the demonstrator application the advantages are overwhelming. We will here itemise the chief positive features of VHS:

(a) The procedure for interpolation of the distribution function from particles to phase space grid results in very low noise levels in the current/charge density fields.

(b) The VHS algorithm makes very efficient use of particles. In PIC codes the distribution function is expressed in some average sense by the density of the (weighted) simulation particles. With VHS the same quantity is expressed as a floating point number. It is at once apparent that to achieve the same degree of accuracy a PIC code will need far more particles than a VHS code. Even worse, for many plasma simulation problems $\delta F \ll F_0$, and in this case the signal to noise ratio of PIC codes becomes very bad indeed.

(c) The VHS algorithm has a time-varying phase box and is able to accommodate flux of phase fluid across the boundary. The dynamic particle population of VHS codes conveys huge advantages relative to PIC codes with their fixed populations of simulation particles. Time is not wasted following particles that are no longer of interest. A good example of this is the demonstrator application which is a wave particle interaction problem in an inhomogeneous medium. The VHS code automatically restricts itself to resonant particles, whereas a PIC code would end up with a sizeable fraction of nonresonant particles.

(d) The VHS code offers good control over velocity space and good diagnostics, in that the distribution function is immediately available.

(e) In any problem where F_0 is not small on the phase box boundary, PIC codes will generate large "end errors." VHS codes normally assume that $F = F_0$ outside the phase box, which is a reasonable approximation. In PIC codes the regions of phase space not filled with particles correspond to $F = 0$, which is a far worse approximation.

13. THE DEMONSTRATOR APPLICATION

The demonstrator application is a space plasma simulation in the VLF band at 3–4 kHz. The code is a simulation of rising and falling frequency emissions triggered by narrow band pulses transmitted by the VLF facility at Siple Antarctica (see the paper by Helliwell and Katsufrakis [12] and numerous papers by the STARLAB group at Stanford). The triggered emissions result from nonlinear electron cyclotron resonance in the equatorial region of the earth's magnetosphere at $L \cong 4.2$. There is extensive literature on this subject, reviewed in [17]. Previous numerical simulations have been LTS PIC codes [8, 9], to which the reader is referred.

In this paper we shall present only the most general features of the simulation, plus some of the latest results from running the code. For full details of the VLF problem the reader is referred to a recent paper by the author in Computer Physics Communications [13]. The triggered VLF emission problem is an excellent one with which to test simulation techniques. The phenomenon is strongly nonlinear as well as being "simple" and well defined. The presence of the active VLF experiment at Siple station enables simulations to be compared directly with experiments—in effect the entire magnetosphere becomes a natural laboratory.

The code has one spatial dimension z, the distance along the $L = 4.2$ magnetic field line. The z grid covers the nonlinear interaction zone and extends a few thousand kilometers either side of the equator. The VLF wavefield is assumed to be a parallel propagating (ducted) whistler wave field, restricted to a bandwidth of about 100 Hz.

In order to simulate emissions with a sweeping frequency the centre frequency of the wavefield is allowed to move freely but with constant bandwidth. This quasi-narrow-band wavefield interacts with an unstable anisotropic distribution of energetic electrons ($\approx$keV). The problem is one of nonlinear electron cyclotron resonance in an inhomogeneous medium, since the resonance velocity $V_{res} = (\omega - \Omega)/k$ is a function of position z due to the magnetic field inhomogeneity and also a function of time due to the sweeping frequency of the emission.

The code has three velocity dimensions. Perpendicular velocity magnitude $V\perp$ is a weak coordinate and may be dealt with in a simplified manner [13]. The important velocity components are V_z (or $V^* = V_z - V_{res}$ $(z, t=0)$) and ψ, the phase of $\mathbf{V}\perp$ relative to base phase ϕ_0.

The phase box covers the nonlinear interaction region centred on the equator $z = -Z_L \to Z_R$. The coordinate $\psi = 0 \to 2\pi$ must clearly be covered. The range of parallel velocity V^* covered by the phase box includes the range of resonant velocities appropriate to the current global wavefield plus several "trapping widths" either side. Clearly when simulating a triggered emission the average frequency changes with time and so must the V^* range. Thus in this problem the phase box is clearly a function of time. The flux of phase fluid across the boundary of the phase box will be highly significant. Particles are constantly falling out of resonance with the wavefield and are no longer of interest. New particles are continuously being swept into resonance with the wavefield. Thus VHS with its dynamic particle population is highly suited to this problem. Indeed PIC codes and Vlasov codes with $F=0$ on the phase box boundary will require enormous numbers of particles in order to successfully simulate the triggered emission problem.

14. BASIC EQUATIONS OF THE VLF SIMULATION

We will here cover the basic equations governing the VLF wave particle interaction problem [13]. Inside the plasmapause the ambient plasma is assumed to consist of a dense cold electron population of density $Ne \cong 400$/cc, plus a hot tenuous component that is anisotropic and provides the relatively few nonlinear cyclotron resonant electrons. At VLF frequencies the ion population may be assumed to be immobile.

The ambient magnetic field $B_z(z)$ is taken to be a parabolic function of z about the equator,

$$B_z(z) = B_z(0)\beta = B_z(0)(1 + 0.5Xz^2). \tag{17}$$

It is worth noting that the parabolic form of the inhomogeneity is critically important and totally determines the character of the wave particle interaction process.

For a narrow band wpi problem we first require the definition of a base frequency ω_0, a base wave number $k_0(z)$, and a base phase $\phi_0(z, t)$,

$$\phi_0(z, t) = \omega_0 t - \int^z k_0(z)\, dz. \tag{18}$$

The narrow band whistler wavefield may then be described by a dimensionless complex amplitude $\tilde{R}(z, t)$, where the phase of $\tilde{R}$ equals the phase of the perpendicular electric field $\mathbf{E}\perp(z, t)$ relative to the base phase, ϕ_0, and

$$\tilde{R} = Re^{i\phi}. \tag{19}$$

Maxwell's equations plus the linearised equations of motion of the cold electrons furnish the dimensionless field equation, which is a simple advective equation of the form

$$\left(\frac{\partial}{\partial t} + Vg\frac{\partial}{\partial z}\right)\tilde{R} = -\frac{\omega_0 Vg}{k_0}\tilde{J} - \gamma(|\tilde{R}|)\tilde{R}, \tag{20}$$

where Vg is the whistler group velocity and $\tilde{J}$ is the complex dimensionless resonant particle current. The last term in Eq. (20) is a phenomenological loss term. It represents "nonlinear unducting loss" and other loss mechanisms. When amplitudes reach nonlinear levels the resonant particle current $\tilde{J}$ will radiate into unducted modes and wave energy will escape from the duct. This is a very complex problem and will require a full 3D code to simulate it. Another saturation mechanism is believed to involve velocity space diffusion due to electrostatic waves, since the nonlinear wave particle interaction process drives the plasma to a state in which it is unstable against electrostatic waves. This is also a very difficult problem to simulate.

The Particle Equations of Motion

A complex perpendicular velocity may be defined by

$$\tilde{V}\perp = Vx + iVy; \qquad V\perp \equiv |\tilde{V}\perp| \tag{21}$$

and a perpendicular velocity phase ψ defined by

$$\psi = \arg(\tilde{V}\perp) - \phi_0. \tag{22}$$

A dimensionless parallel velocity V^* is defined by

$$V^* = V_z - V_{res}(z), \tag{23}$$

where $V_{res}(z)$ is the electron cyclotron resonance velocity at ω_0 and is

$$V_{res} = (\omega_0 - \Omega(z))/k_0(z). \tag{24}$$

The equations of motion now reduce to the dimensionless form

$$\dot{\psi} = k_0 V^* \tag{25}$$

$$\dot{V}^* = -\frac{Rk_0 V\perp}{\omega_0}\cos(\psi - \phi) + Q_0 \tag{26}$$

$$\delta\dot{W} = -RV\perp\cos(\psi - \phi), \tag{27}$$

where δW is the change in particle energy. The quantity $Q_0(z)$ is the inhomogeneity factor which is mainly proportional to field gradient dB_z/dz but has a term in cold plasma gradient dNe/dz. Thus Q_0 is closely proportional to z.

The Resonant Particle Current $\tilde{\mathbf{J}}$

The dimensionless resonant particle current $\tilde{J}$ may be shown to be given by the following integral [13]

$$\tilde{J}(z, t) = k_1 \int_0^\infty \{F_0' V\perp^2\} Js(V\perp)\, dV\perp, \tag{28}$$

where

$$Js = \int_0^{2\pi} \int_{V_1^*}^{V_2^*} e^{i\psi}\, \delta W(z, t, V\perp, \psi, V^*)\, dV^*\, d\psi. \tag{29}$$

The quantities V_1^*, V_2^* are the limits of the coordinate V^* in the simulation box. The term F_0' is the appropriate gradient of the unperturbed distribution function $F_0(\mu, W)$ that drives the whistler instability; i.e.,

$$F_0' = \left[\frac{\partial F_0}{\partial W} + \frac{2}{\omega_0}\frac{\partial F_0}{\partial \mu}\right]_{W,\mu}, \tag{30}$$

where the energy W is given by

$$W = (V\perp^2 + (V_{res}(z) + V^*)^2)/2 \tag{31}$$

and the magnetic moment μ is given by

$$\mu = V\perp^2/2\beta; \qquad \beta = B_z(z)/B_z(0). \tag{32}$$

We thus see that F_0' is a function of $V\perp$, z, and the centre frequency $\bar{f}$ of the current wavefield. The functional dependence of F_0' on these three parameters is very critical in determining the emission triggering behaviour of the code. One approach to the problem is to define a full function $F_0(\mu, W)$ analytically, and then calculate F_0' as required. It has been found, however, to be cheaper and more convenient to define F_0' directly. In this simulation we express F_0' as a linear/quadratic function of parallel resonant energy. So

$$F_0' = F_0'(V\perp, z = 0, t = 0)\bar{\gamma} \tag{33}$$

$$\bar{\gamma} = 1 + \alpha_1 q + \alpha_2 q^2, \tag{34}$$

where

$$q = [(V_{res}(z) + V^*)^2 - V_{res}(0)^2]/2 \tag{35}$$

and α_1, α_2 may be functions of $V\perp$.

18. APPLICATION OF THE VHS FORMALISM TO THE VLF SIMULATION PROBLEM

The problem at hand concerns *narrow band* wave particle interaction, and this allows certain simplications to be made. We first note that the complex field $\tilde{R}$ advects at a velocity Vg. We thus set up a spatial *field grid* $(z_r^l, l = 1, Nr)$, where $Nr \sim 600$ and the grid separation $\Delta Zr = Vg\, \Delta t$, Δt being the simulation timestep. The field $\tilde{R}$ is only defined at the z_r^l and at each timestep the value of $\tilde{R}$ advects to the right to the next grid point. All particles of interest have velocity V_z close to $V_{res}(0)$. As far as the evaluation of $\delta W(V\perp, V^*, \psi, z, t)$ is concerned it is a legitimate approximation to advect the SP's at $V_{res}(0)$. Hence we may establish a spatial *particle grid* $(z_J^l, l = 1, N_J)$, where $N_J = 512$ and the grid separation $\Delta Z_J = -V_{res}(0)\, \Delta t$. Simulation particles are only defined on this grid, and at each timestep the entire set of SP's at one spatial grid point is moved leftwards to the next one. During the implementation of the field push and particle push equations it is necessary to cross-interpolate between these two spatial grids. This is readily accomplished using precomputed weighting coefficients.

Evaluation of the Current $\mathbf{J}$ *on the Particle Grid*

We first note that the coordinate $V\perp$ in Eqs. (28), (29) is relatively "weak." Significant nonlinear particles have a pitch angle range from 45–65°, so the integral in Eq. (28) may be replaced by a summation over $N_{v\perp}$ discrete values, where $N_{v\perp}$ can be quite small. Most of the physics is secured with $N_{v\perp}$ in the range 2–5. Larger values of $N_{v\perp}$ are of course desirable but very expensive in terms of computing time. Similarly the integral over coordinate ψ can be replaced by a discrete summation over N_ψ values, where N_ψ is in the range 16–20, and the integral over V^* replaced by a discrete summation over N_{v^*} in the range 30–60. Now the quantity δW is evaluated by integrating $\dot{W}$ along particle trajectories in the $\tilde{R}$ field. Along these trajectories $V\perp$ undergoes only small changes and to a good approximation may be put constant. Thus there is no need to invoke the VHS interpolation procedure for the coordinate $V\perp$. The same goes for coordinate z since SP's are only defined at grid points z_J^l. We thus set up a separate 2D phase space box in coordinates ψ, V^* at each grid point z_J^l and for each value of $V\perp_i$. The current $\tilde{\mathbf{J}}_l$ at z_J^l is then obtained from

$$\tilde{\mathbf{J}}_l = k_1 \sum_{i=1}^{N_{v\perp}} V\perp_i^2 F_0'(z_J^l, V\perp_i, f)\, Js(V\perp_i, z_J^l), \tag{36}$$

where

$$Js(V\perp_i, z_J^l) = d\Gamma \sum_{j=1}^{N_\psi} \sum_{k=1}^{N_{v^*}} e^{i\psi_j}\, \delta W(V\perp_i, \psi_j, V_k^*, t, z_J^l), \tag{37}$$

and

$$d\Gamma = \Delta\psi\, \Delta V^* \tag{38}$$

is the area of one grid square.

The VHS formalism is thus applied to $N_{v\perp} \cdot N_j$ separate (ψ, V^*) planes, where δW is evaluated on each phase space trajectory. It is easily shown that the flux of particles in the ψ, V^* plane is divergence-free and thus the phase fluid is incompressible in these new variables.

Simulation Control

The bandwidth and the amplitude of the wavefield must be controlled as the simulation progresses. The real saturation mechanisms are nonlinear unducting and diffusion due to electrostatic waves. Both of these effects increase rapidly when wave amplitudes reach nonlinear levels (>1 pT) at which nonlinear particle trapping occurs. In the code, saturation has to be modelled phenomenologically by a damping term $-\gamma\tilde{R}$ that is a rapidly increasing function of wave amplitude. It was found that the bandwidth of the wavefield tends to increase without limit as the simulation proceeds. The simulation code, however, can only accommodate a limited bandwidth of order 100 Hz, depending on the memory and computer power available. The solution is as follows. At every timestep the wavefield is spatially DFT'd and the central frequency $\bar{f}$ is determined. The field is then filtered to the desired bandwidth with a filter centred on $\bar{f}$. Simultaneously the centre of the V^* axis of the phase box is adjusted so that it corresponds to the resonance velocity at frequency $\bar{f}$.

Simulation Diagnostics

The VLF simulation code can output a wide variety of diagnostics as follows:

(a) Wave amplitude R in picoteslas and wave phase ϕ as functions of position z and time t.

(b) Components of resonant particle current **J** parallel to $\mathbf{E}_\perp$ (termed Jr) and perpendicular to $\mathbf{E}_\perp$ (Ji).

(c) The spatial DFT of the wave field, either as individual spectra or in the form of a f/t plot.

(d) A time DFT of the field $\tilde{R}$ exiting from the simulation box, presented as an f/t plot. This is done for several frequency resolutions.

(e) Phase-averaged distribution function $\bar{F}$ at various z, t.

(f) *Ginosurf* plots of δW in the ψ, V^* plane for any z, t, $V_\perp$.

(g) Plot of average frequency $\bar{f}$ against time.

(h) Calculation of average electrostatic growth rate as a function of z at any time—plus the bandwidth of the unstable electrostatic wavefield.

19. NUMERICAL RESULTS

In this paper we shall only present the results for one run of the VHS/VLF code. This is a simulation of the triggering of a rising frequency VLF emission ("riser") by a CW pulse from the Siple VLF facility in Antarctica. Simulation data are set out in Table I.

The simulation is driven by two pitch angle "beams," for reasons of economy. These are of roughly equal "strength" and close together at high pitch angles $\sim 60°$.

Figure 5 shows wave amplitude $R(z, t)$ in picoteslas at a time of 525 ms. This corresponds very well to the profile for a quasi-static riser generation region as described in [14]. The ducted VLF wave particle interaction problem is seen to have a considerable excess of input power—the profile is hard up against the saturation level for $z > 500$ km. In the real system nonlinear unducting loss will provide the dominant saturation mechanism. Future simulations should seek to model the loss mechanisms more precisely. The low amplitude end of the generation region is at $z = -360$ km and corresponds to a point of zero net inhomogeneity as described by Helliwell [15].

Also plotted on the graph is the wave number bandwidth that is unstable to Langmuir (electrostatic waves), expressed as a fraction of the maximum bandwidth in the simulation. The third curve is an estimate of the average electrostatic wave growth rate (in hertz) within this unstable band. This reaches about 30 Hz (1600 dB/s) over the

TABLE I

Input Data for Siple Riser Simulation

L shell no. = 4.2
$\Omega e = 18.87$ kHz
$\Pi e = 179$ kHz
Cold plasma density $Ne = 400$/cc
Pulse frequency (initial) = 5048 Hz
Pulse length = 89 ms
Initial amplitude $B_{in} = 0.1$ pT
Saturation amplitude $B_{max} = 4.95$ pT
Trapping frequency at B_{max}; $F_{tr} \cong 39$ Hz
Simulation bandwith = 94 Hz
Linear growth rate at equator = 135 dB/s
$N_v^* = 30$; $N_\psi = 16$; $N_j = 512$; $N_r = 603$; $Nv\perp = 2$;
Total no of simulation particles $N_t = 578$K to 627K;
$V\perp_1 = 2.8$ (pitch angle = 64.4°)
$V\perp_2 = 3.2$ (pitch angle = 67.3°)
$(V\perp^2 F_0')_{V\perp_1} = k \cdot 3.5$
$(V\perp^2 F_0')_{V\perp_2} = k \cdot 4.0$
$\alpha_1 = \alpha_2 = 0$

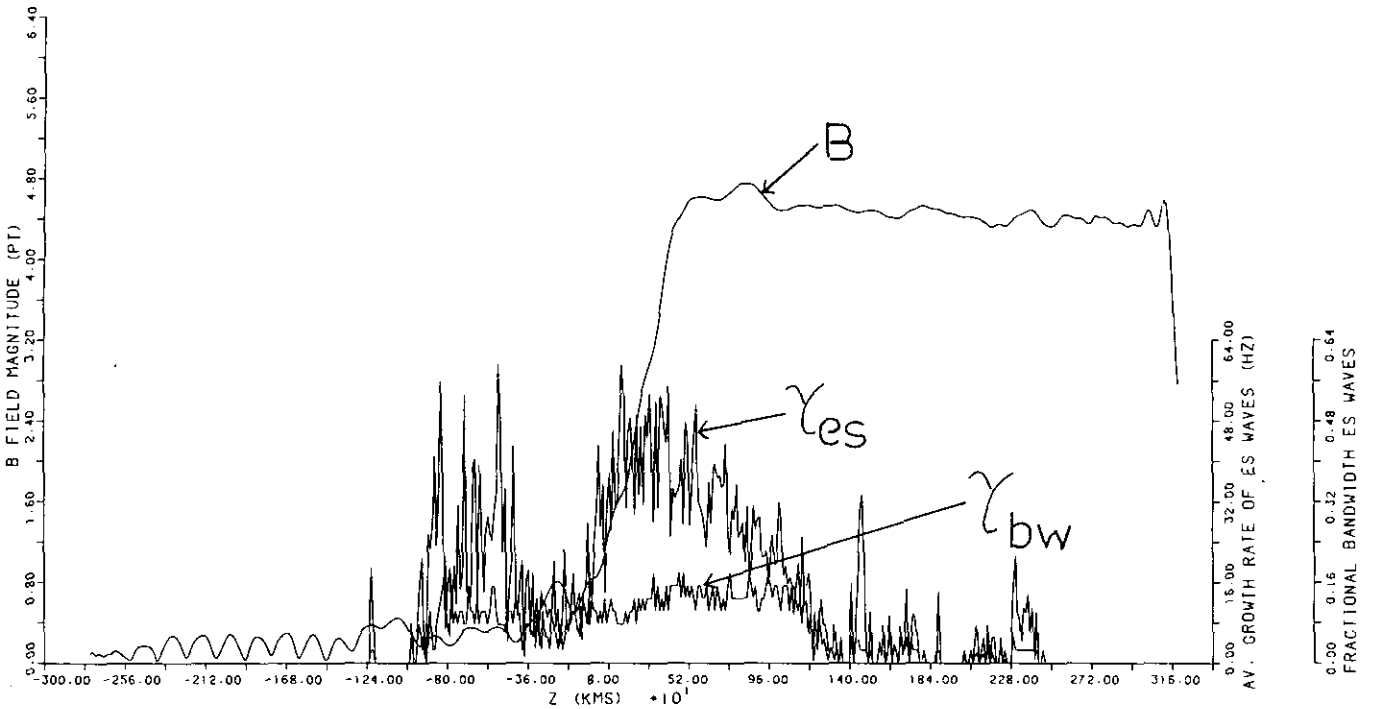

FIG. 5. Wave profile in pT (curve B) of a rising frequency emission. The jagged line (BW) is the fractional bandwidth unstable to electrostatic waves. The curve γ_{es} is the averaged electrostatic growth rate (in hertz) within this unstable band.

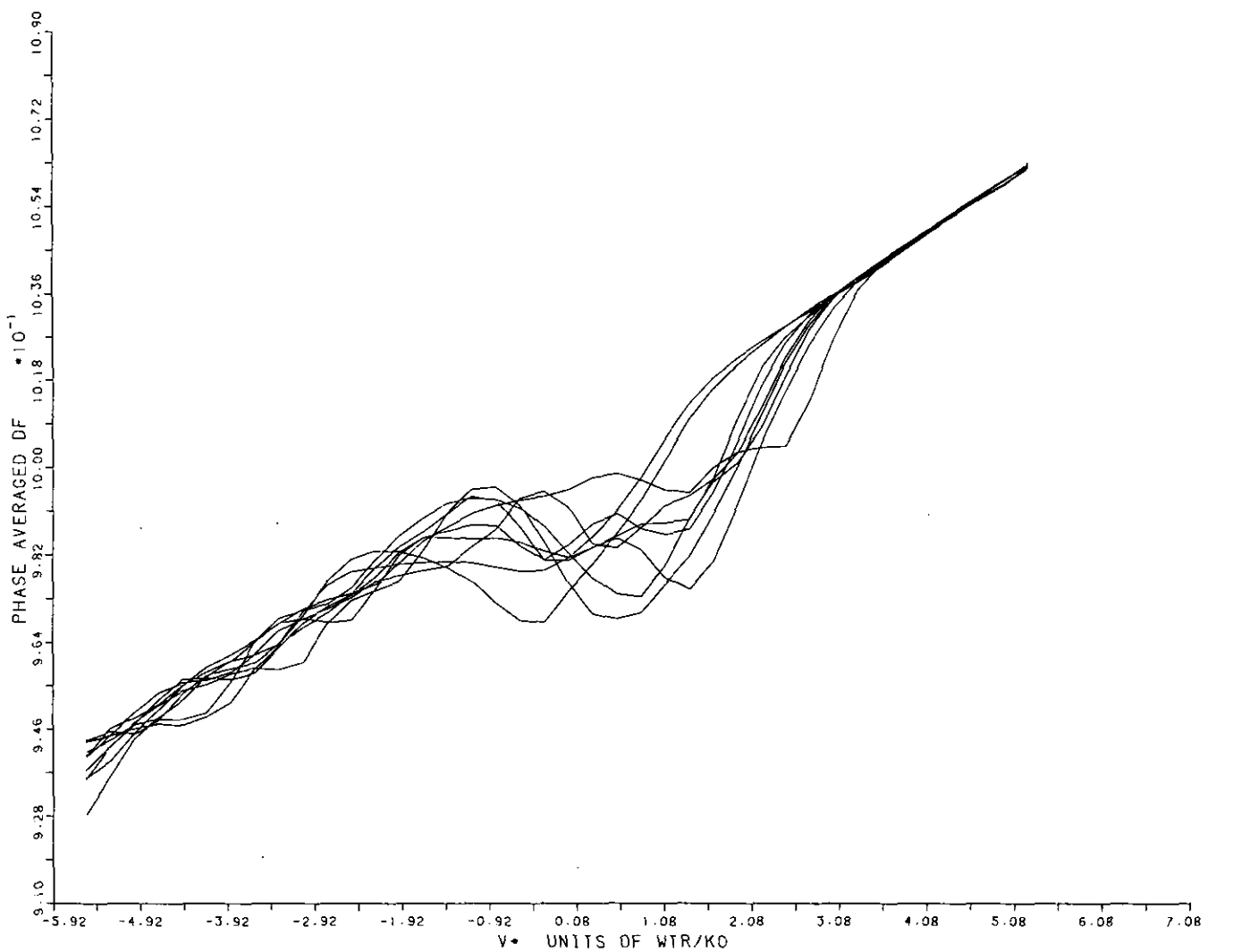

FIG. 6. Plots of phase averaged distribution function $\bar{F}$ as functions of V^* for values of z spaced across the simulation region. These curves are for $V\perp = V\perp_i$; $t = 1200\ \Delta t$.

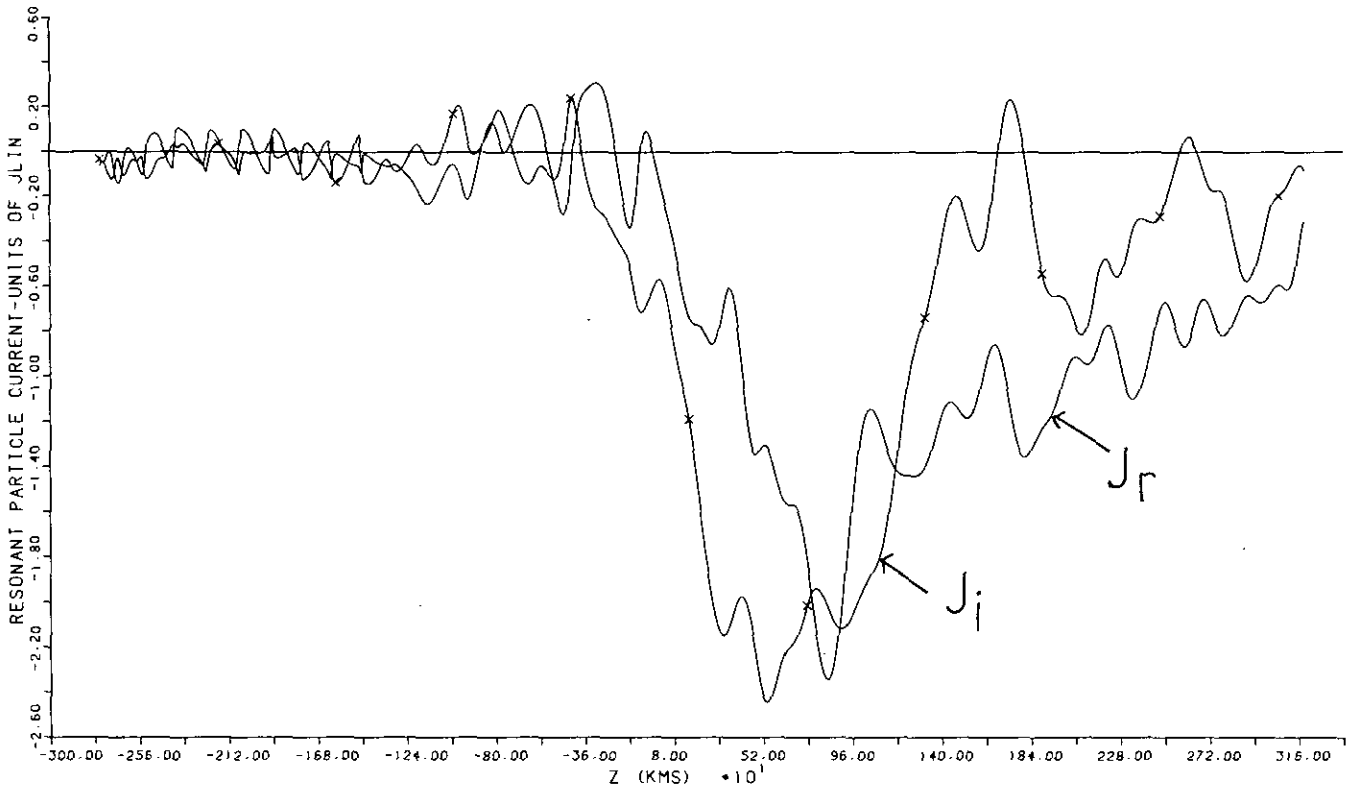

FIG. 7. Plots of resonant particle current $\tilde{J}$ in dimensionless units, plotted against z in kilometers. The quantity Jr is the component in phase with $\mathbf{E}\perp$, while J_i is that in phase with $\mathbf{B}\perp$.

strongly nonlinear part of the generation region, i.e., from $+1000$ to -1000 km. Clearly, since Langmuir waves will have small group velocities, electrostatic wave amplitudes will reach high levels and cause significant diffusion of the phase-averaged distribution function, thus acting as an additional saturation mechanism. The origin of this electrostatic instability is easily understood. Particle trapping in a negative inhomogeneity results in a "hole" in the distribution function [13]. On the "far" side of this hole the gradients of the phase averaged distribution function will give electrostatic instability. This is confirmed by Fig. 6 which plots phase averaged distribution function $\bar{F}$ at $V\perp_1$

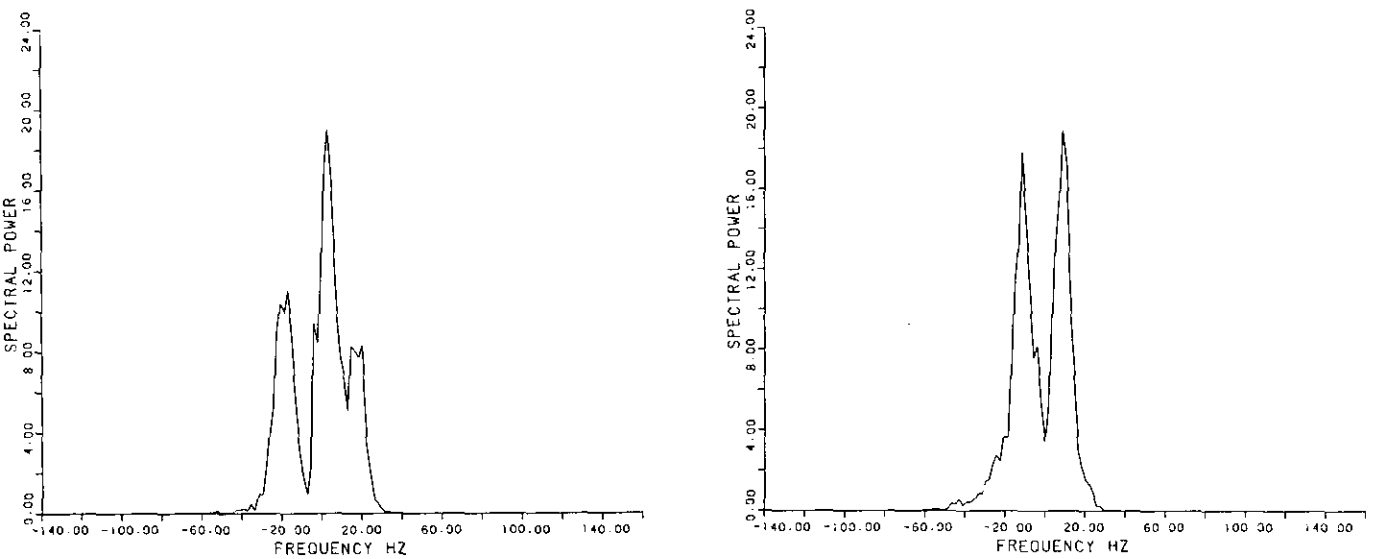

FIG. 8. Wave number spectra of the simulation field $\tilde{R}(z, t)$ at $t = 1.063$ s and $t = 2.126$ s. Note the marked resonant sideband at 40 Hz separation.

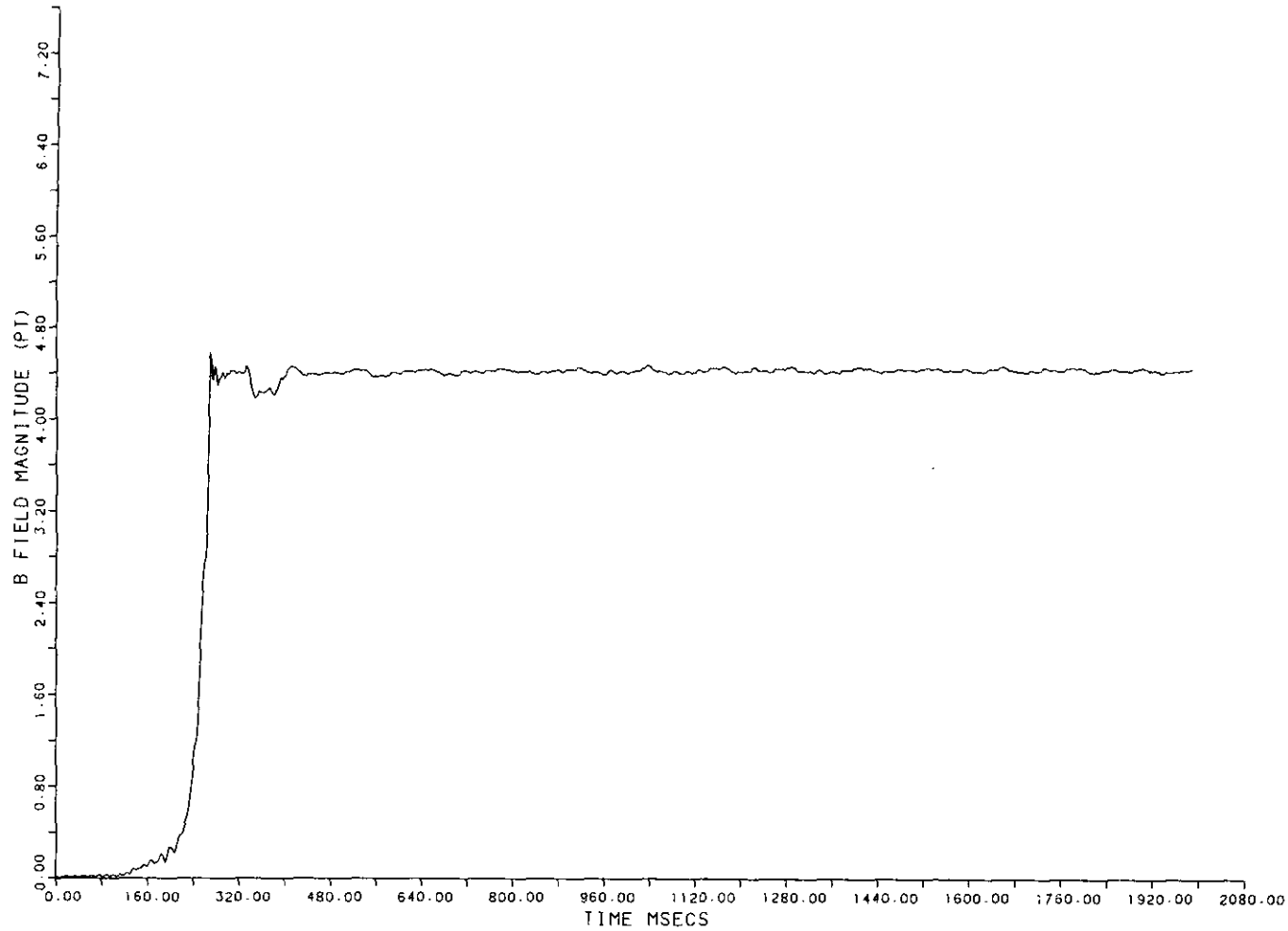

FIG. 9. Wave amplitude in picoteslas exiting from the simulation region.

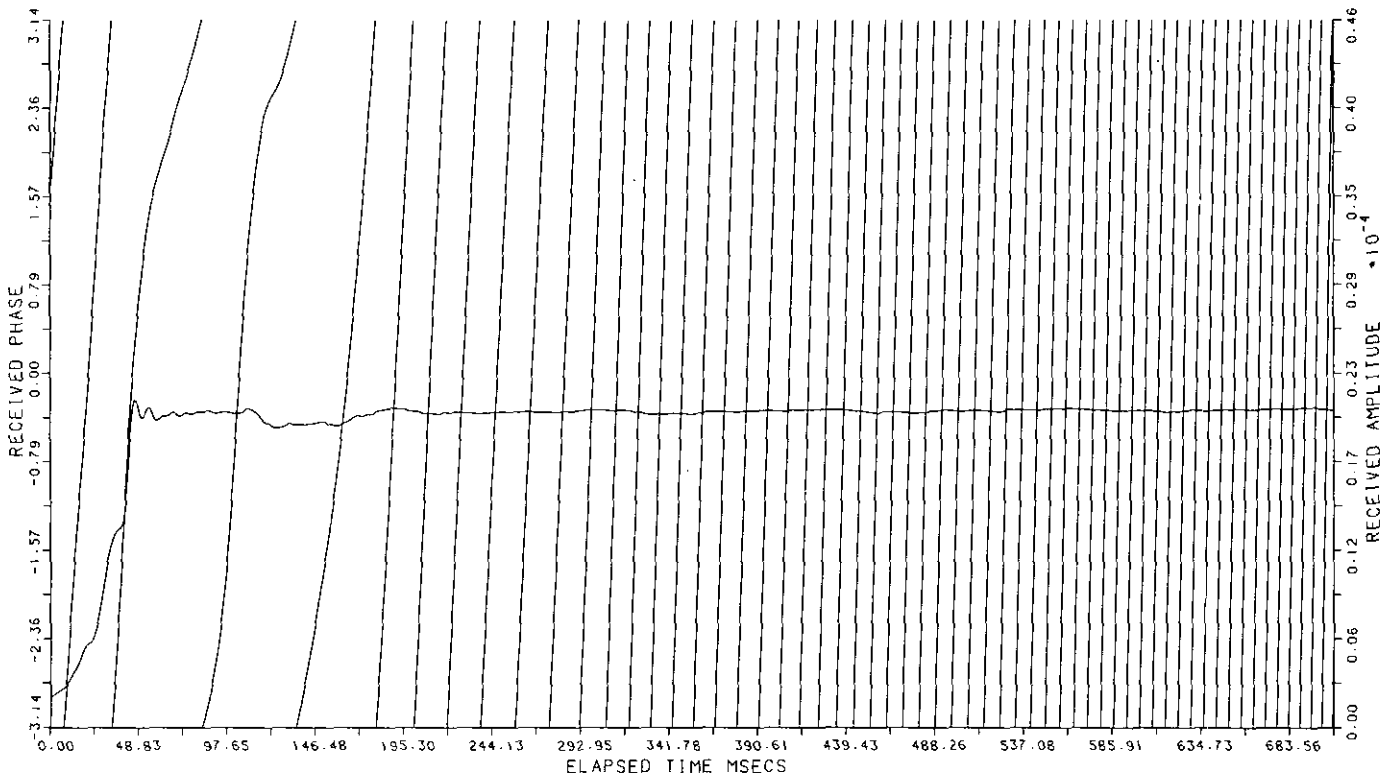

FIG. 10. Additional phase ϕ of the wave field exiting from the simulation region. This is a monotonically increasing function of time going as $\sim t^2$.

as a function of V^* for various z, at a time $t = 1200\ \Delta t$. The depressions in $\bar{F}$ correspond to trapped particles.

Figure 7 plots resonant particle currents Jr and Ji as functions of z at $t = 525$ ms. Again these curves agree with computations of the generation regions of riser emissions [14]. The magnitude and phase of the resonant particle current are as expected from simple trapping consideration [13]. The oscillatory components in Jr, Ji are directly due to the sidebands present in the wavefield.

Figure 8 shows the wave number spectra of the simulation field $R(z, t)$ at $t = 1.06$ and 2.12 s. A strong sideband is observed at a separation of 40 Hz, which is close to the trapping frequency F_{tr} at the saturation amplitude. It was shown in [16] that VLF waves are upper sideband unstable in negative inhomogeneities when nonlinear trapping occurs, the maximum instability being at a separation $\sim F_{tr}$. Since the riser generation region is entirely in the region of negative inhomogeneity, these spectral structures are as expected. Indeed the mechanism for frequency change in a riser may be regarded as being a successive transfer of wave energy to the next upper sideband.

Figure 9 plots the wave amplitude $R(z, t)$ in picoteslas exiting from the simulation region. The amplitude increases rapidly and exponentially to the saturation level and stays there. In reality observed amplitude behaviour shows slower exponential growths starting from very low amplitudes. This probably involves effects due to broadband unducted turbulence and nonlinear unducting.

The additional phase ϕ exiting from the simulation box is shown in Fig. 10. This increases monotonically with time as t^2, as expected from a riser.

Figure 11 plots spatial DFTs of the field $\tilde{R}(z, t)$ in the simulation box every 12 ms, giving an f-t plot of the whole simulation. The equivalent frequency resolution of each DFT is 1.86 Hz. The riser starts off as closely spaced sidebands and then becomes a succession of discrete rising

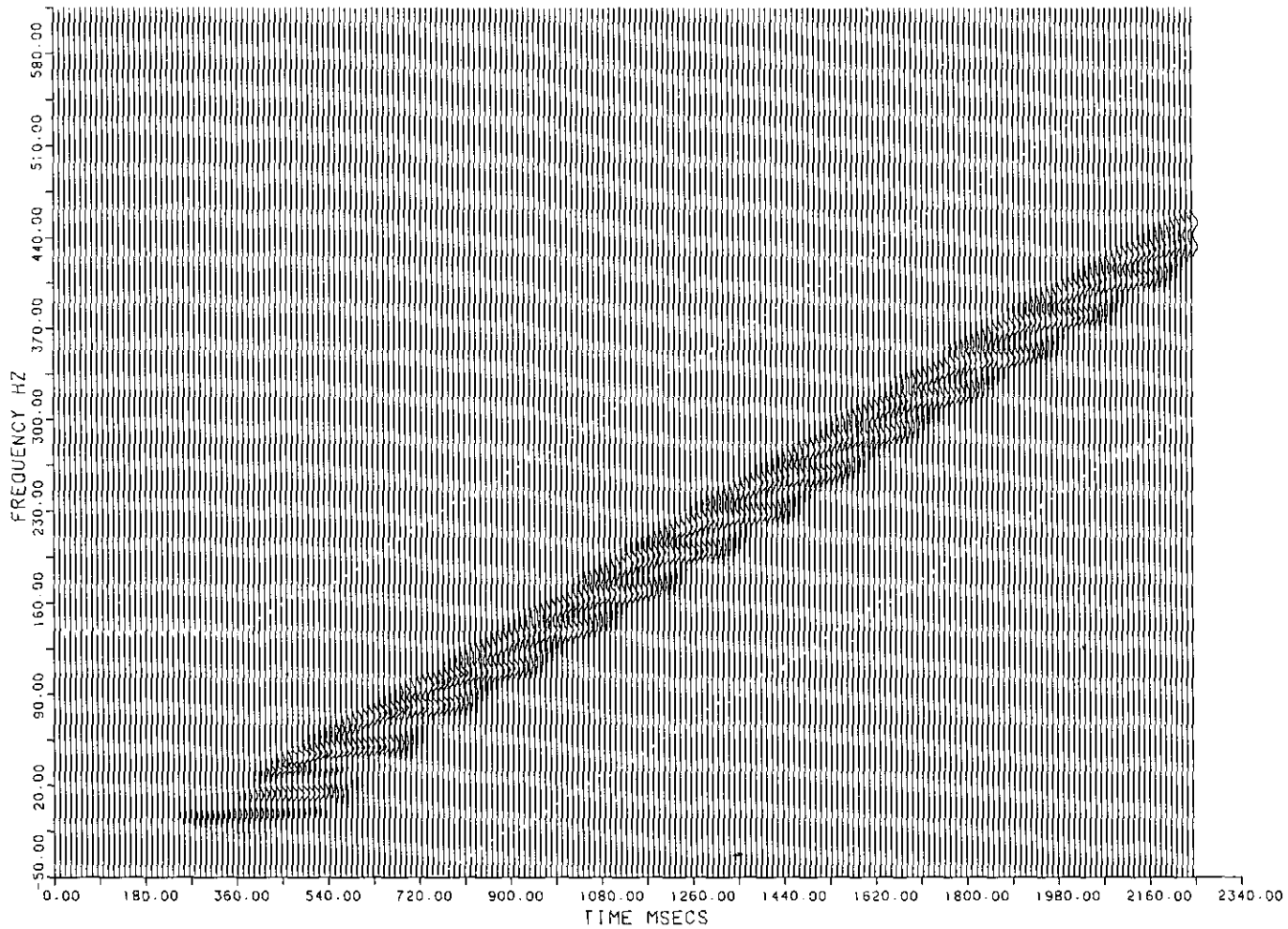

FIG. 11. Spatial DFTs of simulation wavefield, with equivalent resolution of 1.86 Hz, presented every 12 ms to give an f-t history of the simulation field $\tilde{R}(z, t)$. The emission consists of successive rising frequency elements with separation ~ 40 Hz.

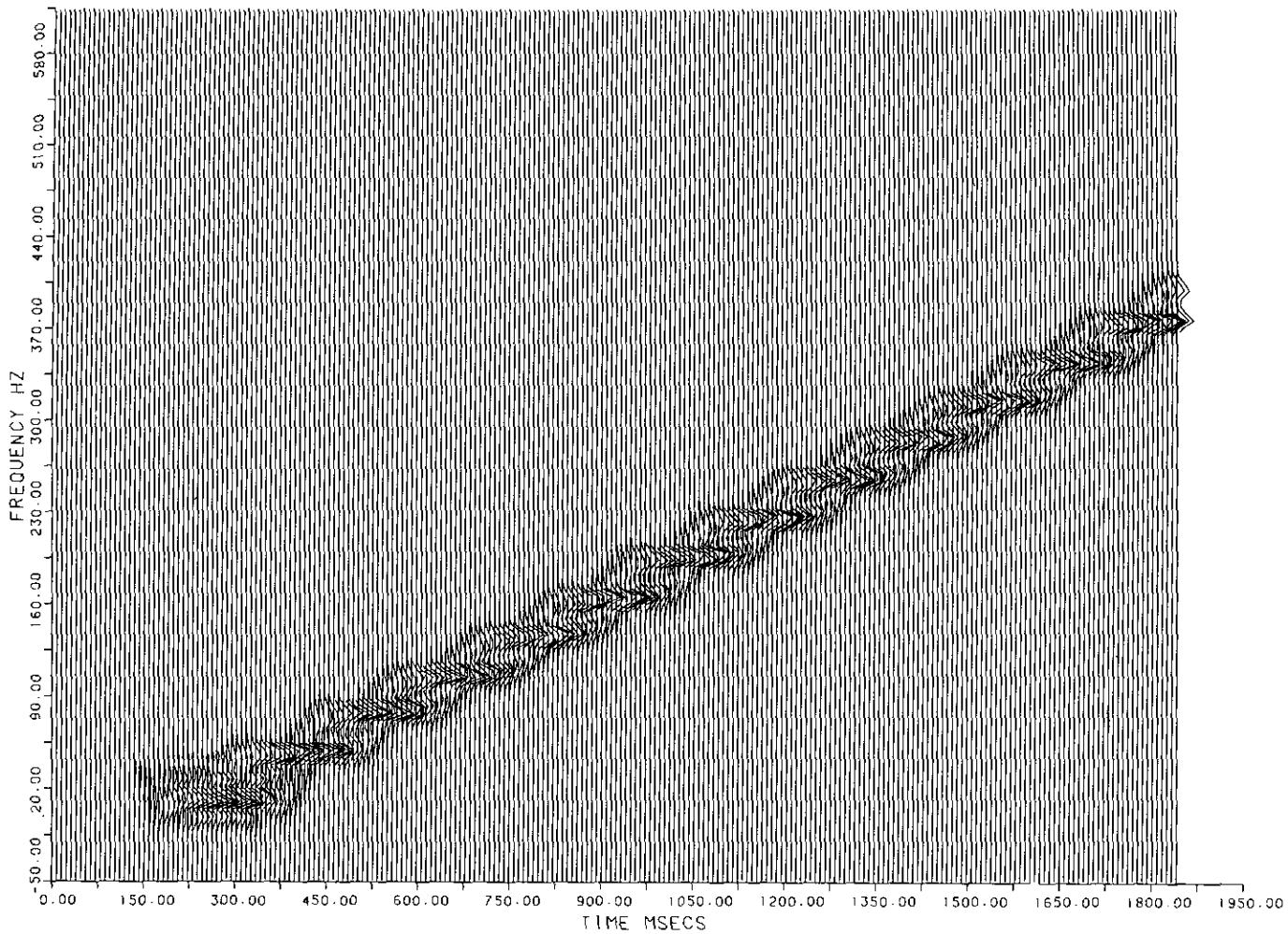

FIG. 12. A true f-t plot of the time series $\tilde{R}(Z_R, t)$ emerging from the simulation region. Frequency resolution is 5.64 Hz. The emission now appears as a succession of constant frequency pulses with a somewhat variable separation of order 40 Hz.

elements, giving a curious ropelike appearance to the plot. The slope of the riser is about 300 Hz/s, in reasonable agreement with observations. It should be noted that when simulating a riser or faller the code periodically divides out accumulated frequency shifts for reasons of stability and numerical accuracy. Certain quantities such as Vg, $V_{\text{res}}(0)$, k_0, and the spatial grid are not adjusted to take into account large changes in frequency.

Figure 12 is a true f-t plot applied to the time series $\tilde{R}$ exiting from the simulation box. The frequency resolution in this case is 5.64 Hz. The emission is seen to consist of a series of short pulses with somewhat variable frequency separations of order 40 Hz. The original triggering pulse is completely swamped by the powerful emission. The triggering pulse is usually more apparent in the observations.

Figure 13 is a sample contour plot of δW in the ψ, V^* plane at $t = 1800\,\Delta t$, $V\perp = V\perp_1$, and at $z = 34\,\Delta Z_j$. The group of trapped particles with large positive δW near $V^* = 0$, $\psi = 2.5$ is clearly visible.

A large number of further simulations have been performed, including NAA triggered emissions, simulations of small frequency shifts with NAA MSK transmissions, Siple sideband experiments, and whistler-triggered emissions. These results will appear in future publications.

20. COMPUTER SCIENCE CONSIDERATIONS

All the computationally intensive parts of the VHS/VLF code are able to be vectorised, including the interpolation of δW from the particles to the phase space grid. The most expensive part of the code are: (a) particle push (about 40%); (b) interpolation of δW from particles to grid (30%); (c) integration of δW over velocity space to obtain $\tilde{J}$ (20%); (d) normalisation of ψ (5%); and (e) field push, insertion of new particles, particle control (5%). With 600 K simulation particles the time for one timestep on the IBM3090/600E is about 8 s, with a whole simulation taking about 6 h on this machine.

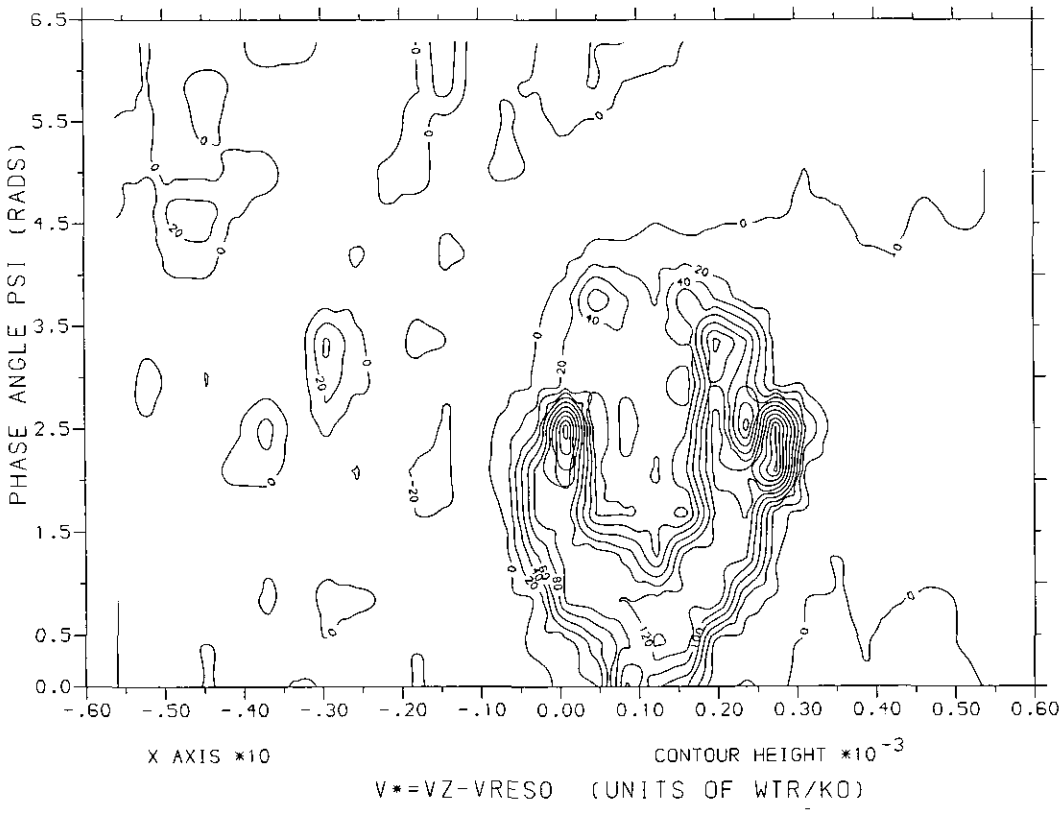

FIG. 13. Contour plot of δW in the ψ, V^* plane for $V\perp = V\perp_1$, $t \approx 1800\,\Delta t$, $z = 34\,\Delta Z_j$. The contour labels are δW in dimensionless units. The trapped particle bunch with large positive δW is clearly seen near $V^* \approx 0$, $\psi = 2.5$.

The VHS/VLF code has a parallelism of $Nj = 512$ in its computationally intensive parts and is thus well suited for implementation on massively parallel computation engines. A linear processor array could be mapped onto the spatial grid, and the amount of interprocessor communication would be quite small relative to the amount of computation being done by each processor.

Regarding VHS codes in general, the particle push, the interpolation procedure, and the integration of δF over velocity space should always vectorise. Particle push and integration of δF will clearly be easily parallelised. Parallelisation of the interpolation procedure may be achieved, although not so easily as in the narrow-band VLF case. For a K-fold parallelism the phase box would have to be divided into K overlapping equally sized regions such that the total boundary area was minimised. Particles would need to be assigned to each region, and then interpolation could take place separately in each region. Grid points on the boundaries between regions would require special treatment involving communication between adjacent processors.

21. CONCLUSION

A general system for the numerical simulation of collision-free plasmas has been presented. The method, termed VHS, is far more efficient than PIC codes particularly when $\delta F \ll F_0$. The algorithm is stable, tolerant of distribution function fine structure, and does not require artificial diffusion of the distribution function. The unique feature of the algorithm is the *interpolation* of distribution function from particles to a fixed phase space grid. This enables one to accomodate a flux of phase fluid into and out of the phase space simulation box and hence have a dynamic population of simulation particles. For some problems this can confer huge advantages.

In this paper VHS is applied to the triggered VLF emission problem, but it is expected that the method will be universally applicable to any collision-free plasma.

ACKNOWLEDGMENTS

The author thanks the Southampton University Computing Services and Atlas Centre at Rutherford Laboratory for their frequent assistance. The author thanks SERC for grants to finance computer usage at Rutherford Laboratory.

REFERENCES

1. R. W. Hockney and J. W. Eastwood, *Computer Simulation Using Particles* (Adam Hilger, Bristol, 1988).
2. J. Denavit, *J. Comput. Phys.* **9**, 75 (1972).
3. C. Z. Cheng and G. Knorr, *J. Comput. Phys.* **22**, 330 (1976).

4. J. P. Boris, *Proc. 4th Conf. Numerical Simulation of Plasmas, 1970*, p. 3.
5. J. P. Boris and D. L. Book, *J. Comput. Phys.* **20**, 397 (1976).
6. G. Chanteur, in *Computer Simulation of Space Plasmas* (Reidel, Dordrecht, 1985), p. 279.
7. P. Bertrand, A. Ghizzo, M. Shoucri, M. Feix, and E. Fijalkow, in *Proceedings, 13th Conf. Numerical Simulation of Plasmas, Santa Fe, NM, 1989.*
8. J. Denavit, *Phys. Fluids* **28** (9), 2773 (1985).
9. A. Simon, S. Radin, and R. W. Short, *Phys. Fluids* **31** (12), 3649 (1988).
10. W. S. Lawson, *J. Comput. Phys.* **61** (1), 51 (1985).
11. M. Kotschenreuther, *Phys. Abstr.* **33** (9), 2107 (1988).
12. R. A. Helliwell and J. P. Katsufrakis, *J. Geophys. Res.* **79**, 2511 (1974).
13. D. Nunn, *Comput. Phys. Commun.* **60**, 1 (1990).
14. D. Nunn, *Planet. Space Sci.* **32**, 325 (1984).
15. R. A. Helliwell, *J. Geophys. Res.* **72**, 4973 (1967).
16. D. Nunn, *Planet. Space Sci.* **34**, 429 (1986).
17. Y. Omura, D. Nunn, H. Matsumoto, and M. Rycroft, *J. Atmos. Terr. Phys.* **53**, No. 5, 351 (1991).
18. Y. Omura and H. Matsumoto, *J. Geophys. Res.* **87**, 4435 (1982).
19. Y. Omura and H. Matsumoto, *J. Geomagn. Geoelectr.* **37**, 829 (1985).
20. H. Okuda and C. Z. Cheng, *Comput. Phys. Commun.* **14**, 169 (1978).
21. T. Tajima and F. W. Perkins, *Proceedings, 1983 Sherwood Theory Meeting, University of Maryland, 1983*, p. 219.
22. T. Tajima, *Computational Plasma Physics* (Addison–Wesley, Redwood City, CA, 1989), p. 225.
23. M. Kotschenreuther *et al.*, in *Plasma Physics and Controlled Nuclear Fusion Research*, IAEA, *Vienna, 1990*, Paper D-4-16.
24. M. Kotschenreuther, in *1990 Sherwood Theory Conference*, College of William and Mary, Williamsburg, VA, 1990, Paper 3C6.
25. J. A. Beyers, in *Proceedings, Fourth Conference on Numerical Simulation of Plasmas, NRL, Washington, DC, 1970*, p. 496.
26. A. M. Dimits and W. W. Lee, in *Proceedings, 12th Conference of the Numerical Simulation of Plasmas, LLNL, Livermore, CA, 1987, Paper* PW23.
27. D. C. Barnes and R. A. Nebel, *Bull. Am. Phys. Soc.* **36**, 2433 (1991).